P-wave velocity and Gamma density from multisensor core logger and its relation with deep-water sedimentary facies of Quaternary Mass-Transport Complex, Southern continental slope of Campos Basin

Anderson Gomes de Almeida, Petrobras/E&P-EXP, Renato Oscar Kowsmann, Petrobras/CENPES, Alberto Garcia Figueiredo Jr/Departamento de Geologia e Geofísica, UFF

Abstract

The aim of this study is to understand the physical properties of deep-water mud facies. Eleven jumbo piston cores, collected in a mass transport complex in the region of the southeastern group of canyons of the continental slope of the Campos Basin, were analyzed. P-wave velocity and Gamma density obtained from Geotek multi-sensor core logger as well as sedimentological description of the cores were used. It is propose a descriptive sedimentary facies scheme with genetic implications for deep-water deposits. Seven facies were distinguished: (I) hemipelagic mud; (II) matrix-supported mud-clast conglomerate; (III) distorted stratified mud; (IV) clast-supported mud-clast conglomerate; (V) mud-blocks; (VI) structureless mud; and (VII) parallel-laminated mud and sand intercalation.

The hemipelagic mud facies corresponds to the Holocene drape and has the lowest V_p and Gamma density values and the highest porosity. Although dispersion of Gamma density and V_p data in diagrams, it is possible to distinguish fields for each type of facies with partial overlapping. The complexity of facies classification using physical properties is aggravated by the burial compaction. To remove this effect the layers were decompacted to zero meters depth. The values of $V_{p(0)}$ and $\sigma_{(0)}$ at the surface were calculated for each facies type using linear regression. The MTC facies have higher values of $V_{p(0)}$ and $\sigma_{(0)}$ and lower values of porosity$_{(0)}$, indicating compaction and loss of fluids during transport before their final burial.

Introduction

In this study, 11 Jumbo Piston Cores (JPC) were collected in a Mass-Transport Complex (MTC) located in the region of the Southeast Group of Canyons of the continental slope of the Campos Basin (Figure 1).

The canyons of the Southeast Group, which comprise Goitacá, Tupinambá, Temiminó, Tamoio and Tupiniquim canyons (Brehme, 1984, Reis, 1994, Viana *et al*., 1999). The canyons have U-shaped smooth cross-section, and their troughs contain large mass-transport deposits, with abundant scattered blocks (Almeida & Kowsmann, 2016).

The submarine canyons, and several removal scars, are associated to mass-transport process (Kowsmann *et al*., 2002) largely controlled by surface geology and geostrophic currents (Vianna *et al*., 1998). Those processes occurred on the slope mainly in the periods of relative low sea level (Kowsmann & Viana, 1992). In addition to erosive and depositional processes, the shape of the sea bottom is controlled by geologic structures such as faults and salt domes (Almeida & Kowsmann, 2016).

The main mass-transport complex features are slump scars, anfitheatre scar, and scarps of planar failure (Almeida *et al.*, 2015). According to Tripsanas *et al.* (2008) there is no comprehensive descriptive scheme to describe mass-transport deposits at the scale of piston cores and this has resulted in misinterpretation of failure deposits and overuse of the genetic term ‘debris flow’.

The aim of this study is to understand the relationship between the P-wave velocity and Gamma density obtained by the Geotek Multi-Sensor Core Logger (MSCL) and sedimentary facies of the cores in order to aid the comprehension of the rheological behavior of submarine mass-transport.

Data and Method

The research vessel Fugro Explorer carried out the JPC collection. The coring process was customized to the soil conditions revealed by seabed PiezoCone Penetration Tests (PCPT) performed prior to deployment of the sampling tool.

The JPC was lowered until a trigger weight comes in contact with the seafloor. The JPC then free falls 2 m to its final penetration depth. A piston inside the JPC stays at the same depth relative to the trigger position, increasing sample quality as the core is cut. The JPC and core were then brought back to the vessel and the deployment steps were reversed to recover the tool. The JPC was outfitted with a beacon to determine the position before triggering (FUGRO, 2012).

The cores were removed from the top of the JPC to preserve the integrity of the seabed sediments. The cores were retrieved in a 102 mm diameter PVC liner and then cut into 0.9 m sections, capped and transferred to the MSCL lab onboard for P-wave velocity (V_p) and Gamma density (σ) measurements.

In the P-wave velocity logger a short P-wave pulse is produced at the transmitter, propagates through the core and is detected by the receiver. Pulse timing software is used to measure the travel time of the pulse with a

resolution of 50 ns. The distance travelled is measured as the outside core diameter with an accuracy of 0.1 mm. After suitable calibration procedures have been followed the P-wave velocity can be calculated with a resolution of about 1.5 m/s. The accuracy of the measurements will largely depend on any variations in liner wall thickness (GEOTEK, 2014).

A Gamma ray source and detector are mounted across the core on a sensor stand that aligns them with the centre of the core. A narrow beam of collimated gamma rays is emitted from a Caesium-137 source with energies principally at 0.662 MeV. These photons pass through the core and are detected on the other side. At this energy level the primary mechanism for the attenuation of gamma rays is by Compton scattering. The incident photons are scattered by the electrons in the core with a partial energy loss. The attenuation, therefore, is directly related to the number of electrons in the Gamma ray beam (core thickness and electron density). By measuring the number of transmitted Gamma photons that pass through the core unattenuated the density of the core material can be determined. To differentiate between scattered and transmitted photons the Gamma detector system only counts those photons that have the same principal energy of the source. To do this a counting window is set which spans the region of interest around 0.662 MeV (GEOTEK, 2014).

Results and Discussion

Eleven JPCs were used to propose a descriptive sedimentary facies scheme with genetic implications for deep-water deposits. Seven facies were distinguished: (I) hemipelagic mud; (II) matrix-supported mud-clast conglomerate; (III) distorted stratified mud (as secondary lamination, Caddah *et al.*, 1994); (IV) clast-supported mud-clast conglomerate; (V) mud-blocks; (VI) structureless mud; and (VII) parallel-laminated mud and sand intercalations (transported by tractive currents). Being that Facies II to VI are MTC facies.

The relationship between the sedimentary facies described and the physical properties obtained by MSCL profiles was verified as follows.

In order to understand the MTC facies rheological behavior resulting from the strain suffered during transport, the V_p and σ logs were used. In Figure 2, the values of V_p versus σ were plotted in a scatterplot with the facies plotted with different symbols. This scatterplot shows a clear separation of the hemipelagic mud facies values that constitutes the Holocene drape (Caddah *et al.*, 1998) and presents reduced values of V_p and σ.

The values of V_p and σ present a high correlation (R^2 = 0.9607) when fitting a quadratic equation curve. The following equation is obtained: $V_p = 398.65\ \sigma^2 - 1107.7\ \sigma + 2248.5$.

The MTC facies have higher values of V_p and σ as a result of the consolidation during mass transport strain and stress. Otherwise the Facies IV (parallel-laminated mud and sand intercalation) is typical of contourites and presents the highest values of density and V_p due to the presence of siliciclastic sands (it can also be constituted by bioclastic fragments) that have V_p and σ higher than clay minerals.

Although the V_p and σ are scattered (Figure 2) it is possible to distinguish fields for each facies, though these sometimes overlap.

The difficulty of facies classification using physical properties is aggravated by the burial consolidation. To remove this effect the layers were decompacted to seabed surface (depth = 0 m). The values of $V_{p(0)}$ and $\sigma_{(0)}$ at the surface were calculated for each facies by linear regression. In this way it is be possible to compare the $V_{p(0)}$ and $\sigma_{(0)}$ values for each facies at the same burial level. The seabed surface was chosen for comparison because it represents roughly the depositional environment conditions. The linear regression curve of V_p and σ, in function of burial, for each facies was obtained (Figure 3).

For Facies III it was verified that the σ and V_p of the JPC-11 have different fitting curves from the other JPCs (Figure 3, E and F). While Facies VI (Figure 3, L and M) have three fitting curves, grouped as JPC-3 and JPC-4; JPC-7 and JPC-10; JPC-6, although the latter has no V_p profile.

In order to integrate the results, the scatterplots of $V_{p(0)}$ versus $\sigma_{(0)}$ and $porosity_{(0)}$ versus $\sigma_{(0)}$ of each facies are presented in Figure 4 (A and B, respectively).

It is observed that the Facies I presents the lowest values of $V_{p(0)}$ and $\sigma_{(0)}$, and the highest values of $porosity_{(0)}$. The MTC facies have higher values of $V_{p(0)}$ and $\sigma_{(0)}$ and lower values of $porosity_{(0)}$, which indicates greater consolidation and loss of water during mass transport.

Among the MTC facies, facies V, although it has high $\sigma_{(0)}$ (1.67 g/cc), it has a very low $V_{p(0)}$ (1480.89 m/s). It is possible to interpret that the relatively high $\sigma_{(0)}$ is due to the pre-consolidated mud blocks and the low $V_{p(0)}$ to the lack of contact between the blocks and to the high water content of the muddy matrix.

The facies II and IV present intermediate values of $V_{p(0)}$ and $\sigma_{(0)}$. Facies II has $V_{p(0)}$ equal to 1,492.46 m/s and $\sigma_{(0)}$ 1.57 g/cc, while facies IV presents slightly higher values, $V_{p(0)}$ equal to 1496.88 m/s and $\sigma_{(0)}$ equal to 1.65 g/cc. These relative higher values are related to the greater amount of pre-consolidated mud-clasts that in turn present greater contact between each other. The pre-consolidated mud-clasts in contact, and the lack of porous matrix, favor the propagation of the P wave.

Facies III, with the exception of the JPC-11, has a high value of $\sigma_{(0)}$ (1.69 g/cc) and the highest value of $V_{p(0)}$ (1,518.52 m/s). The internal shearing is responsible for the expulsion of part of the interstitial water. This strain mechanism is typical of the base of landslides and is interpreted as responsible for the highest values of $Vp_{(0)}$.

The Facies III observed in JPC-11 has lower $V_{p(0)}$ (1490,03 m/s) and $\sigma_{(0)}$ (1.52 g/cc), and the highest porosity value (60%) of MTC facies. These data indicate that this type of sediment underwent fluidization with water incorporation in the internal shear surfaces.

Facies VI presents two fitting curves for $V_{p(0)}$ and $\sigma_{(0)}$ separated into two groups of JPC. Facies VI of the JPC-7 and JPC-10 presents intermediate values of $V_{p(0)}$ (1494.41 m/s) and $\sigma_{(0)}$ (1.65 g/cc). Probably these sediments constitute intermediate portions of plastic flows or free translation in MTC front portion (see Figure 1 for morphological context). Facies VI of the JPC-3 and JPC-4 presents very high values of $V_{p(0)}$ (1494.41 m / s) and $\sigma_{(0)}$ (1.65 g/cc). This facies can be interpreted as a flow that has undergone homogenization, probably a plastic flow in the MTC frontal portion, or else it can be related to large pre-consolidated blocks translated with the mass flow. The homogeneous texture of the Facies VI could also be an earthquake effect.

Conclusions

The linear regression of V_p and σ versus burial depth determined the $Vp_{(0)}$ and $\sigma_{(0)}$ values at seabed surface. It was observed that Facies I of the Holocene drape has the lowest values of V_p and σ, and the highest porosity. In contrast, the MTC facies have higher values of V_p and σ and lower values of porosity, indicating greater consolidation and loss of water during the mass transport. The overconsolidation observed in the MTC facies is caused by the combination of mass transport strain and burial effects. Facies VII (not an MTC) presents high values of σ and V_p due to the presence of interbedded sand.

Facies V and Facies VI, of JPC-3 and JPC-4, present relative high V_p and σ due to overconsolidation. Thus they are interpreted as having been generated by elastic strain, that is, from rock fall and sliding of large blocks.

The high-viscosity cohesive debris flow is represented by Facies II and IV. The Facies III (except JPC-11), with high $Vp_{(0)}$ and $\sigma_{(0)}$ values, can be interpreted as base of slump where intensive shear bands generate secondary lamination.

The low viscosity and fluid fluxes are represented by the Facies VI of JPC-6 and by the Facies III of JPC-11. Both characterized by relative low values of $Vp_{(0)}$ and $\sigma_{(0)}$.

Acknowledgments

The authors would like to gratefully acknowledge to Petrobras for support and to ANP for authorization of data use by the first author's doctoral degree at Universidade Federal Fluminense, Programa de Pós-Graduação em Dinâmica dos Oceanos e da Terra (DOT). The authors gratefully acknowledge the reviewer Dr. Fernando Freire for their thoughtful comments. Special thanks are due to Petrobras marine geology management, survey team mates and crew of R/V Fugro Explorer.

References

ALMEIDA, A. G. 2015. Geomorfologia e sismoestratigrafia de alta resolução dos complexos de transporte de massa e estabilidade do talude da região do Grupo Sudeste de Cânions da bacia de Campos, RJ. Dissertação de Mestrado. Universidade Federal Fluminense. 127p.

ALMEIDA, A. G. & Kowsmann, R. O. 2016. Geomorphology of the continental slope and São Paulo Plateau. In: Geologia e Geomorfologia, regional environmental characterization of the Campos basin, Southwest Atlantic. Rio de Janeiro: Elsevier, Habitats, v.1, 33-66 p.

BREHME, I. 1984. Vales submarinos entre o banco de Abrolhos e Cabo Frio, Rio de Janeiro. Dissertação de mestrado, Universidade Federal do Rio de Janeiro. 116 p.

CADDAH, L. F. G., KOWSMANN, R. O., & VIANA, A. R. 1994. Laminação secundária em sedimentos escorregados: um exemplo do Pleistoceno da Bacia de Campos. Bol. Geociências da Petrobrás, v. *8,* n. 2/4, 421-427 p.

CADDAH, L. F. G., KOWSMANN, R. O., & VIANA, A. R. 1998. Slope sedimentary facies associated with Pleistocene and Holocene sea-level changes, Campos Basin, southeast Brazilian Margin. Sedimentary Geology, 115, 1, 159-174 p.

FUGRO. 2012. Jumbo Piston Core. Retrieved from https://www.fugro.com/docs/default-source/Expertise-docs/Our-Services/Geotechnical/jumbo-piston-core.pdf?sfvrsn=0

GEOTEK. 2014. MSCL Manual. Retrieved from http://www.geotek.co.uk/sites/default/files/MSCLmanual.pdf

KOWSMANN, R. O. & VIANA, A. R. 1992. Movimentos de massa provocados por cunhas progradantes de nível de mar baixo: exemplo na Bacia de Campos. Petróleo Brasileiro SA PETROBRAS, Boletim de Geociências, v. 6, n. 1/2, 97-102 p.

KOWSMANN, R. O.; MACHADO , L. C. R.; VIANA, A. R.; ALMEIDA Jr., W.; VICALVI, M. A. 2002. Controls on mass-wasting in deep water of the Campos Basin. 34th Offshore Technology Conference; Houston, Texas. Richardson: Society of Petroleum Engineers. 1-11 p.

REIS, A. T. 1994. O Grupo Sudeste de Cânions e sua Relação com a Progradação do Leque São Tomé, RJ. Dissertação de Mestrado. Observatório Nacional. Rio de Janeiro. 124 p.

TRIPSANAS, E. K.; PIPER, D. J. ; JENNER, K. A. ; BRYANT, W. R. 2008. Submarine mass-transport facies: New perspectives on flow processes from cores on the eastern North American margin. Sedimentology, *55,* 1, 97-136 p.

VIANA, A. R.; ALMEIRA, W.; MACHADO, L. C. 1999. Different styles of canyon infill related to gravity and bottom current processes: examples from the upper slope of SE Brazilian margin. 6th International Congress of the Brazilian Geophysical Society; Rio de Janeiro, Brasil. Sociedade Brasileira de Geofísica. Expanded Abstract 01499.

VIANA, A. R.; FAUGÈRES, J.-C.; STOW, D. A. V. 1998. Bottom-current-controlled sand deposits: a review of modern shallow to deep-water environments. Sedimentary Geology, v. 115, n. 1, 53-80 p.

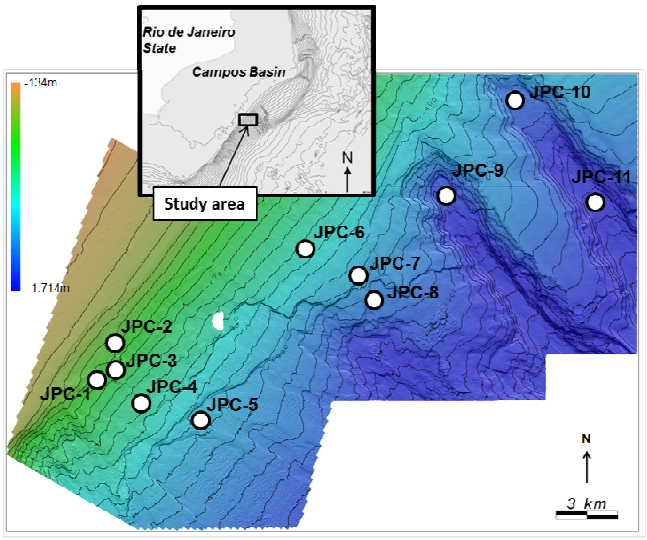

Figure 1 *– Map location of study area.*

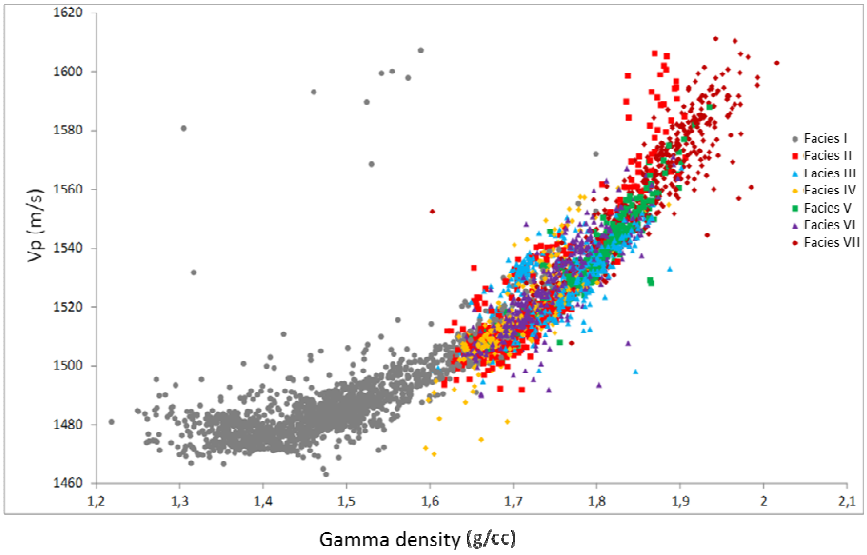

Figure 2 *– Scatterplot Vp versus Gamma density with facies classification.*

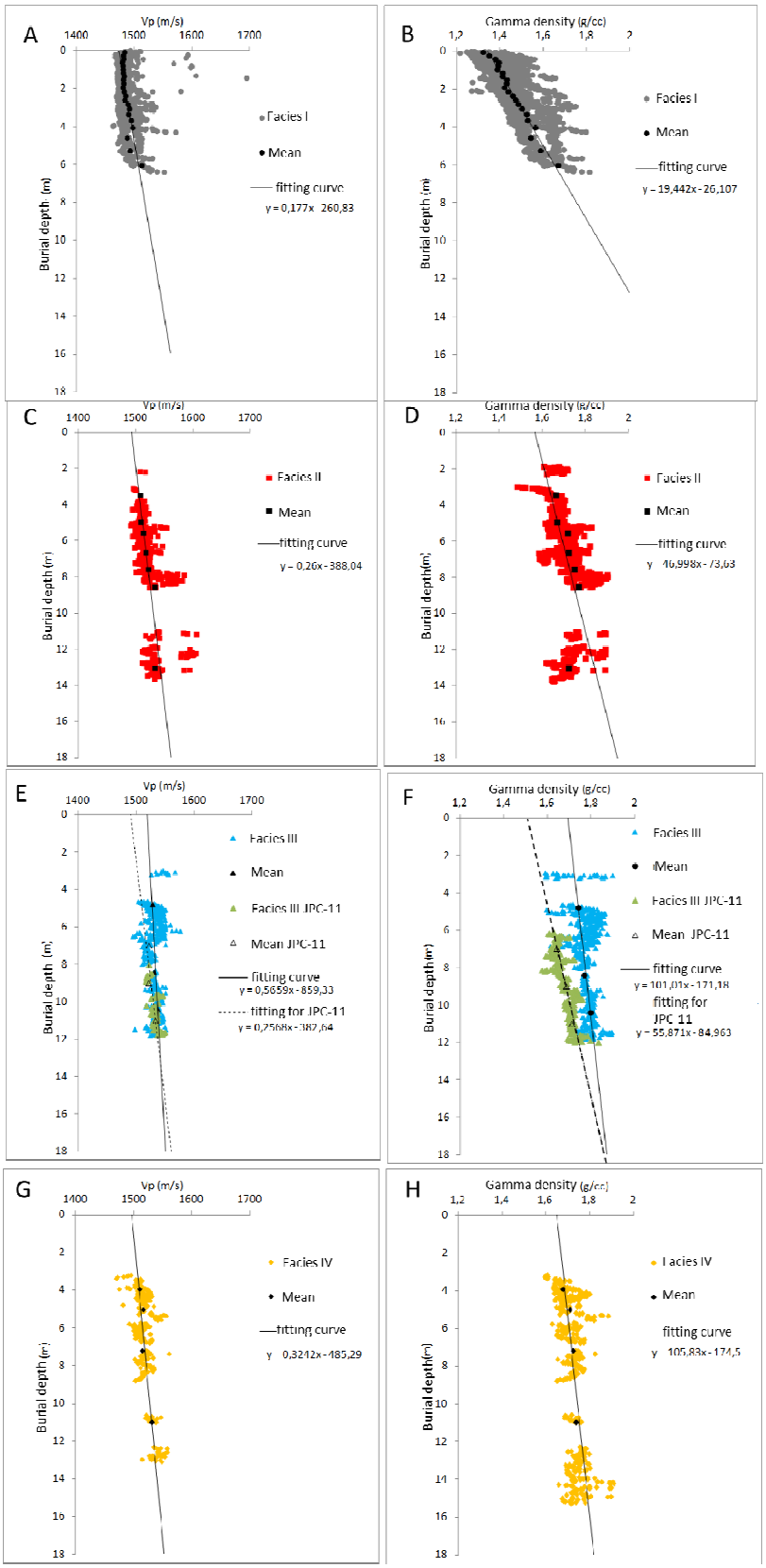

Figure 3 *– Scatterplot Vp versus burial depth and gamma density versus burial depth for each facies.*

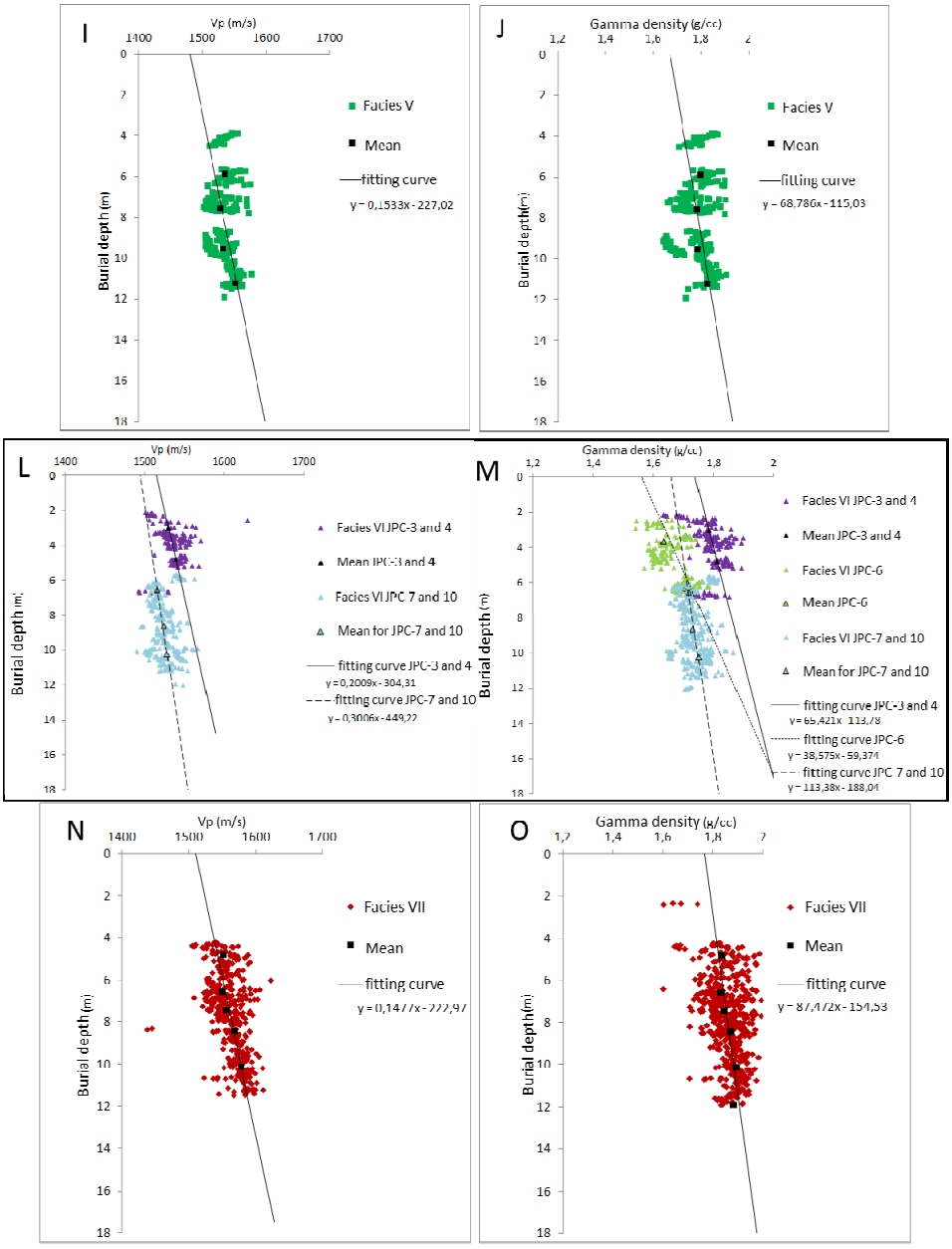

Figure 3 *– (Continued).*

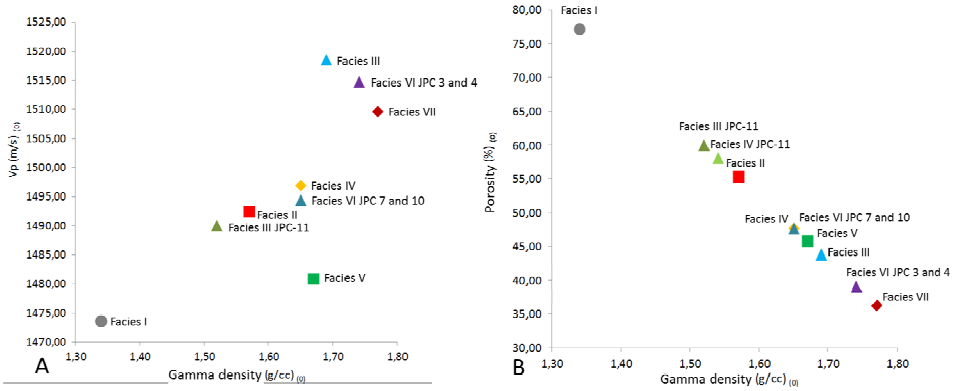

Figure 4 *– A) scatterplot Vp versus gamma density; B) scatterplot Porosity versus gamma density.*